Featured in Physics

Bidirectional Cascaded Superfluorescent Lasing in Air Enabled by Resonant Third Harmonic Photon Exchange from Nitrogen to Argon

Zan Nie,[1,2,*] Noa Nambu,[1] Kenneth A. Marsh,[1] Daniel Matteo,[1] C. Kumar Patel,[1] Chaojie Zhang,[1] Yipeng Wu,[1] Stefanos Carlström,[3] Felipe Morales,[3] Serguei Patchkovskii,[3] Olga Smirnova,[3] Misha Ivanov,[3,†] and Chan Joshi[1,‡]

[1]*Department of Electrical and Computer Engineering, University of California Los Angeles, Los Angeles, California 90095, USA*
[2]*Wuhan National Laboratory for Optoelectronics, Huazhong University of Science and Technology, Wuhan 430074, China*
[3]*Max Born Institute, Max-Born-Strasse 2A, D-12489 Berlin, Germany*

(Received 29 December 2023; accepted 18 June 2024; published 7 August 2024)

Cavity-free lasing in atmospheric air has stimulated intense research toward a fundamental understanding of underlying physical mechanisms. In this Letter, we identify a new mechanism—a third-harmonic photon mediated resonant energy transfer pathway leading to population inversion in argon via an initial three-photon excitation of nitrogen molecules irradiated by intense 261 nm pulses—that enables bidirectional two-color cascaded lasing in atmospheric air. By making pump-probe measurements, we conclusively show that such cascaded lasing results from superfluorescence rather than amplified spontaneous emission. Such cascaded lasing with the capability of producing bidirectional multicolor coherent pulses opens additional possibilities for remote sensing applications.

DOI: 10.1103/PhysRevLett.133.063201

"Air lasing refers to the remote optical pumping of the constituents of ambient air that results in a directional laserlike emission from the pumped region." [1] This remarkable phenomenon of cavity-free air lasing discovered about a decade ago [2] has opened unique opportunities in remote sensing [3], LIDAR, and coherent Raman spectroscopy [4–7], especially if robust backward lasing can be achieved. In all schemes demonstrated so far [1,2,8–23], such backward lasing in atmospheric air has been achieved only by the resonant excitation of atomic species, such as the two-photon excitation of atomic oxygen or nitrogen [1,2,24] or three-photon excitation of atomic argon (Ar) [25] with ultraviolet (UV) lasers. To achieve lasing in atomic oxygen and nitrogen, the molecular oxygen (O_2) and nitrogen (N_2) present in air have to be dissociated first, which induces significant fluctuations of lasing amplitude due to the highly nonlinear intensity dependence of the dissociation process. To avoid such complexity, one needs to rely on the atomic species already present in ambient air, making Ar, the most abundant atomic species in the atmosphere, the best candidate [12]. However, Ar concentration in ambient air is only ~1%, making generation of robust backward lasing in atmospheric air extremely challenging. Here, we solve this problem by using multiphoton excitation of N_2, the most abundant atmospheric species, which significantly enhances the excitation efficiency. The created excitation is then efficiently transferred to Ar via third harmoinc photon exchange between the two species, resulting in robust cascaded two-color lasing in atmospheric air. The photon-mediated energy transfer from N_2 to Ar occurs on a much faster timescale than the collisional transfer from Ar to N_2 in a process known as FLEET [26,27].

The identification of a new physical mechanism responsible for air lasing in the forward and backward directions is central to understanding the key physics involved. Previous studies attributed lasing in pure Ar to amplified spontaneous emission (ASE) [12,23]. However, in experiments carried out under similar conditions, our pump-probe measurement results show that lasing either in pure Ar or in Ar contained in atmospheric air is due to superfluorescence (SF). This is a manifestation of what Dicke called superradiance, i.e., cooperative spontaneous emission [28]. Our measurements show that while the lasing intensity is proportional to the square of the density of excited atoms, both the delay time (τ_D) and duration (τ_R) of the radiated pulses are approximately inversely proportional to the density of excited atom density as expected for SF emission. The condition for pure SF to occur is $\tau_D < T_2$ [29], where T_2 is the dephasing time, which acts to destroy the coherence. Experimentally, in pure Ar, the condition of $\tau_D < T_2$ is easily met. However, in atmospheric air, collisions in atmospheric condition could greatly decrease T_2 leading to the quenching of the SF. The new excitation mechanism we discovered, the third-harmonic photon mediated resonant energy transfer from N_2 to Ar, greatly reduces the characteristic delay time τ_D, allowing bidirectional cascaded SF to occur under atmospheric conditions.

In pure Ar, excitation to the $3d'[5/2]_3$ state occurs via three-photon absorption of the 261 nm radiation as shown in Fig. 1(a). Superfluorescent lasing occurs on cascaded

*Contact author: znie@hust.edu.cn
†Contact author: Mikhail.Ivanov@mbi-berlin.de
‡Contact author: cjoshi@ucla.edu

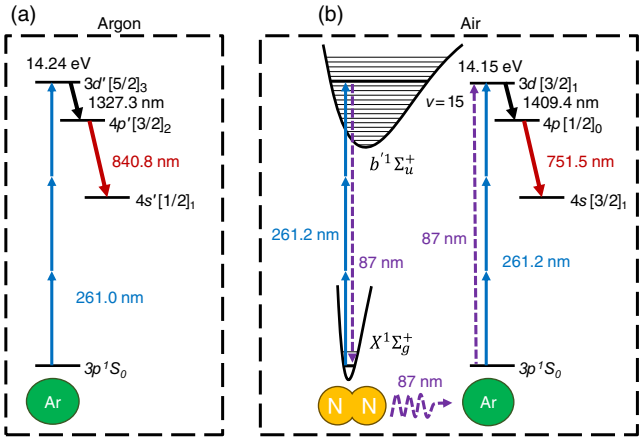

FIG. 1. Relevant transitions of three-photon excitation and cascade lasing in pure Ar and atmospheric air. (a) In pure Ar, the Ar atoms are excited by the 261 nm pump pulse to the $3d'[5/2]_3$ state (14.24 eV) and emit first lasing at 1327.3 nm and second lasing at 840.8 nm. (b) In atmospheric air, the N_2 molecules are excited to the $b'^1\Sigma_u^+$ ($v = 15$) state (14.1551 eV) by the 261.2 nm pump pulse, and emit third-harmonic photons at 87 nm, which is reabsorbed by the surrounding Ar atoms so that the Ar atoms are excited to the $3d[3/2]_1$ state (14.1525 eV) and then emit first lasing at 1409.4 nm and second lasing at 751.5 nm. Note that the center wavelengths of the pump are slightly different: 261.0 nm (Ar) vs 261.2 nm (air) to optimize the pumping of the three-photon resonance.

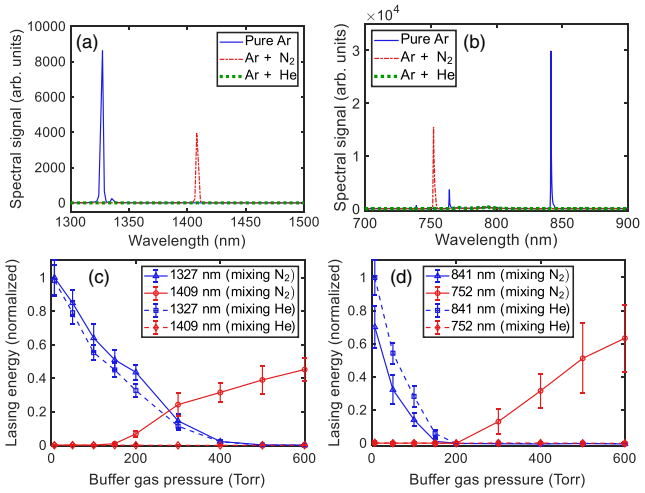

FIG. 2. Evolution of forward cascade lasing spectra when mixing two different buffer gases (N_2 or He) into 7 Torr Ar gas. (a),(b) First and second lasing spectra in conditions of 7 Torr of pure Ar, 7 Torr of Ar mixed with 600 Torr of N_2, and 7 Torr of Ar mixed with 600 Torr of He. (c),(d) Evolution of first and second lasing energy when mixing different ratio of N_2 and He into 7 Torr Ar gas.

1327.3 nm (first lasing) and 840.8 nm (second lasing) transitions. In air, or in Ar and N_2 mixtures, increasing gas pressure increases collisional relaxation of the $3d'[5/2]_3$ state, quenching the cascaded lasing from this state. However, we find that efficient population of the $3d[3/2]_1$ state of Ar atoms can be enabled by initial resonant three-photon excitation of N_2 molecules to the $b'^1\Sigma_u^+$ ($v = 15$) state, followed by ultrafast energy transfer to the $3d[3/2]_1$ state of Ar via emission of third-harmonic photons and reabsorption by the surrounding Ar atoms as seen from Fig. 1(b). This transfer is reminiscent of the ultrafast interatomic Coulombic decay [30–33], where highly efficient resonant transfer of excitation is also mediated by (virtual) photon exchange and occurs on a femtosecond timescale. Importantly, resonantly enhanced emission of third-harmonic photons in N_2 increases with increasing its pressure. Hence, the energy transfer rate to Ar also grows with pressure, counteracting collisional losses. Subsequently, superfluorescent lasing occurs on cascaded 1409.4 nm (first lasing) and 751.5 nm (second lasing) transitions.

The experimental setup is described in the Supplemental Material [34]. First, we focus on the forward cascade lasing. Resonant three-photon absorption can populate several sublevels of $3d$, $3d'$, and even $5s'$ orbitals because of the ~9 THz bandwidth of the 80 fs (FWHM) UV pump pulses. We scan the UV pump wavelength to optimize the cascade lasing signals (see the Supplemental Material [34], Fig. 2). On tuning the pump wavelength to 261.0 nm, we have observed lasing in pure Ar at 1327.3 nm and 840.8 nm. This two-step cascade lasing, shown in Fig. 1(a), proceeds via a common energy level of $4p'[3/2]_2$ with no other intermediate level(s). When replacing pure Ar with laboratory air at atmospheric pressure (typical humidity 50%, about 7 Torr partial pressure of Ar), the first and the second lasing wavelengths switched to 1409.4 nm and 751.5 nm respectively, as shown in Fig. 1(b).

To study the origin of this switching, we added N_2 gas at various pressures to 7 Torr Ar in order to rule out the effect of other gases in air. The first and second lasing spectra in conditions of 7 Torr of pure Ar, 7 Torr of Ar mixed with 600 Torr of N_2, and 7 Torr of Ar mixed with 600 Torr of helium (He) are shown in Figs. 2(a) and 2(b), respectively. Quantitatively [see solid blue and red lines in Figs. 2(c) and 2(d)], as an increasing amount of N_2 is added to 7 Torr Ar gas, the first lasing wavelength switches from 1327.3 nm to 1409.4 nm, and the second lasing wavelength switches from 840.8 nm to 751.5 nm, similar to the case of atmospheric air. The detailed spectral data are shown in the Supplemental Material [34], Fig. 3. When He is added instead of N_2, the 1327.3 nm and 840.8 nm cascade is suppressed, but the 1409.4 nm and the 751.5 nm signals do not appear; see the dashed blue and red lines in Figs. 2(c) and 2(d). Thus, the 1409.4 nm and the 751.5 nm signals arise because of a new pathway enabled by N_2, while the 1327.3 nm and 840.8 nm signals are suppressed primarily by collisional relaxation with increasing density of He or N_2. As shown in Fig. 1(b), the dipole allowed transition

between the ground and $3d[3/2]_1$ states of Ar is resonant with the dipole transition in N_2 between its ground and electronically and vibrationally excited $b'^1\Sigma_u^+$ $(v = 15)$ states, with the detuning below 2.6 meV. Coherence excited by three-photon absorption in N_2 leads to coherent macroscopic emission at the frequency resonant with the excitation of $3d[3/2]_1$ states of Ar, exciting it from the ground state and triggering the 1409.4 nm and 751.5 nm cascade.

To check this hypothesis, we mixed Ar with varying concentrations of O_2, which is also one of the major constituents of air but lacks the required resonance for three-photon absorption of the 261 nm pump light. The observed spectral behavior is similar to that in the Ar-He mixture. This further supports our hypothesis of resonant energy transfer between N_2 and Ar as being responsible for the 1409.4 nm and 751.5 nm cascade lasing in atmospheric air.

We quantified the three-photon absorption cross sections in N_2 and Ar by measuring absorption as a function of pump energy (see the Supplemental Material [34] for details). Our measured value of three-photon (nonlinear) absorption cross section in N_2 of $\sigma(3) = 2.4 \times 10^{-84}\,\mathrm{cm}^6\,\mathrm{s}^2$ is 12 times smaller than the three-photon cross section of $\sigma(3) = 3.0 \times 10^{-83}\ \mathrm{cm}^6\,\mathrm{s}^2$ in Ar. However, there is 78 times more N_2 than Ar in air, making three-photon excitation of N_2 dominant.

We used the pump-probe approach to reveal the temporal dynamics of the forward two air lasing cascades, as shown in Fig. 3(a). Once the 261 nm pump pulse [light blue arrows in Fig. 3(a), energy 20 μJ, peak intensity $4.0 \times 10^{13}\ \mathrm{W/cm}^2$] excites the Ar atoms to the $3d[3/2]_1$ manifold, the ~390 nm probe pulse [blue arrows in Fig. 3(a), energy 60 μJ, peak intensity $5.3 \times 10^{13}\ \mathrm{W/cm}^2$] can one-photon ionize Ar atoms in both $3d$ and $4p$ states, leading to a reduction of gain for both lasing transitions. Figure 3(b) shows the first lasing (black triangle mark) and second lasing (red square mark) signals as a function of pump-probe delay for a 390 nm probe in 1 atm air. When the probe pulse arrives before the pump, the 1409 nm lasing signal is not suppressed because the probe does not affect the lasing process. When the probe arrives just after the pump, both the first and second lasing signals are strongly suppressed due to depletion of the $3d$ and $4p$ state via single-photon ionization by the probe. When the probe pulse is delayed about 20 ps later than the pump, the first lasing signal recovers to its original level, which means that the first lasing signal is emitted within ~20 ps after the pump. Similarly, the second lasing signal is emitted within ~80 ps after the pump. The delay-dependent signals in Fig. 3(b) after the maximal suppression delay are proportional to the time integral of the energy emitted in the first and second lasing steps until the arrival of the probe. Therefore, we can retrieve the pulse profile of the first and second lasing and accordingly their delay time τ_D and pulse durations τ_R by taking the derivatives of the recovery time

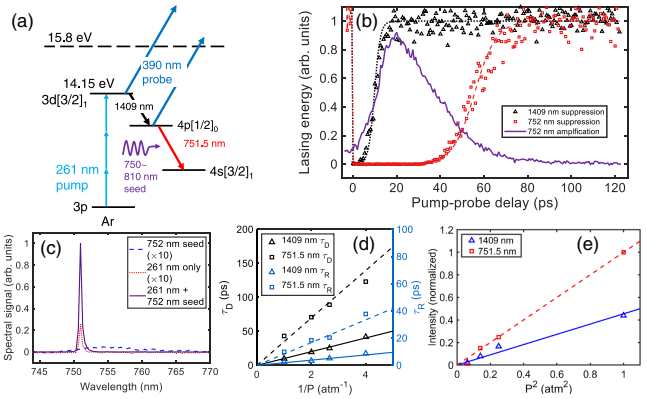

FIG. 3. Pump-probe measurement results in air. (a) Diagram of relevant transitions of pump-probe experiment. (b) The suppression of first lasing (1409 nm, black) and second lasing (752 nm, red), and the amplification of the seed pulse (purple) on second lasing wavelength (752 nm) vs pump-probe delay in 1 atm air. The dotted black and dashed red curves are the best fit to a shifted tanh function. (c) The spectra of second lasing with 752 nm seed only, 261 nm pump only, and both pump and seed (261 nm + 752 nm) at a delay time of 20 ps in atmospheric air. (d) Delay times and pulse durations of first and second lasing signals as a function of the inverse of pressure. (e) Peak intensities of first and second lasing signals compared to the square of pressure. Solid and dashed lines in (d) and (e) show a linear fit to measured data.

of the curves. The dotted black and dashed red curves in Fig. 3(b) show the best fit of the measured data to a hyperbolic tangent function, whose derivative is a sech^2 pulse. The delay time (τ_D) and pulse width (τ_R) for both the first and second lasing pulse at pressures of 1.0, 0.5, 0.375, and 0.25 atm are shown in Fig. 3(d). All of them are inversely proportional to the air pressure. From the measured energy, pulse duration, and spot size, we obtain the peak intensities of the SF as shown in Fig. 3(e), which are proportional to the square of air pressure. Pulse width and delay time being inversely proportional to density and lasing intensity being proportional to the square of the density are the two key signatures of SF [29,35]. Therefore, we confirm that both the first and second lasing in air arise from SF. Since the second lasing is delayed respective to the first lasing, they are cascade SF instead of yoked SF [36].

Furthermore, by using a weak (< 0.1 μJ, peak intensity $< 2.2 \times 10^{10}\ \mathrm{W/cm}^2$) seed pulse centered at 780 nm with sufficient bandwidth covering the spectrum of the second lasing, we can directly see the amplification of the second lasing signal [purple curve in Figs. 3(b) and 3(c)]. The seed is too weak to suppress the first lasing signal, but can amplify the second lasing signal once the $4p[1/2]_0$ level is populated. The rise and fall of this signal reflect the rise and fall of population inversion in the second lasing step. Figure 3(c) shows the spectra of the second lasing with 752 nm seed only, 261 nm pump only, and both pump and

seed (261 nm + 752 nm) at a delay time of 20 ps in atmospheric air. At this delay time, the amplification factor reaches over 100, showing a high optical gain of the second lasing. As expected, the spectrum of the amplified pulse is very narrow compared to that of the seed pulse.

From Figs. 3(b) and 3(d), we can see that the delay time of the 1409 nm first lasing pulse in 1 atm air is ~10 ps. When similar measurements are performed under identical experimental conditions but in 7 Torr of pure Ar, the delay of the dominant 1327 nm first lasing pulse is ~30 ps (see the Supplemental Material [34], Fig. 5). This means that the gain of the 1409 nm lasing in atmospheric air is much larger than that of the 1327 nm lasing in 7 Torr of pure Ar. Also, the 3 times longer buildup time makes the 1327 nm lasing pathway more susceptible to collisional relaxation processes when buffer gases are added [29]. The collision rate between excited Ar atoms and N_2 molecules can be estimated using the formula [37] $\nu_{\mathrm{coll}} = N\sigma\{(8kT/\pi)[(1/M_{\mathrm{Ar}}) + (1/M_{\mathrm{N_2}})]\}^{1/2}$. The cross section was calculated as $\sigma = \pi(r_{\mathrm{Ar}} + r_{\mathrm{N_2}})^2$, where $r_{\mathrm{Ar}} \approx n^{*2}a_0$, with $n^* = 2.99$ is the effective quantum number of the $3d'$ excited state and a_0 is the Bohr radius, and $r_{\mathrm{N_2}} \approx 185$ pm is the radius of the N_2 molecule [38]. This yields an estimated collision time (inverse of collision rate) of 32 ps in 7 Torr of Ar mixed with 600 Torr of N_2, and 25 ps in 7 Torr of Ar mixed with 600 Torr of He, both of which are roughly the same as the delay time of the 1327 nm lasing signal in 7 Torr of pure Ar (~30 ps). This is the reason why the 1327 nm lasing signal quenches in atmospheric air.

Dipole selection rules [39] allow three-photon transitions from states with total angular momentum $J = 0$ (e.g., Ar ground state) to states with either $J = 1$ (e.g., $3d[3/2]_1$) or $J = 3$ (e.g., $3d'[5/2]_3$). However, transitions with $\Delta J = 1$ also have an allowed single-photon excitation pathway. In pure Ar gas at pressures above 1 Torr, excitation to the $3d[3/2]_2$ state is suppressed by interference between three-photon absorption of pump light and single-photon absorption of third-harmonic light [40,41]. This prevents 1409 nm emission and leaves 1327 nm as the most prominent signal, because the third-harmonic single-photon absorption pathway to the $3d'[5/2]_3$ level is forbidden ($\Delta J = 3$) by dipole selection rules. In air, there is a large concentration of N_2, which has a dipole transition from the electronically and vibrationally excited $b'^1\Sigma_u^+$ ($v = 15$) state to ground with an energy defect of < 2.6 meV compared to the energy of the dipole transition from $3d[3/2]_1$ to ground in Ar. At frequencies within the linewidth of the single-photon Ar transition, the refractive index is usually dominated by the contribution from the Ar resonance. In air however, the large concentration of N_2 significantly modifies the refractive index at these frequencies, creating a phase matching condition which enhances third-harmonic generation (THG). The enhanced THG disrupts the balance between the single-photon and three-photon excitation pathways, enabling excitation to the $3d[3/2]_1$ state. This larger population of the $3d[3/2]_1$ state allows lasing on the 1409 nm transition to build up more quickly than on the 1327 nm transition and persist even in the presence of collisions in atmospheric air.

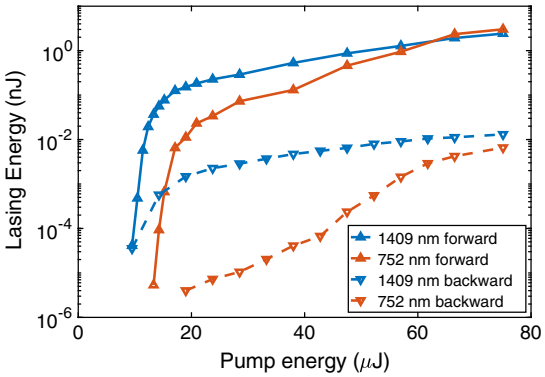

FIG. 4. Comparison of forward and backward cascade superfluorescent lasing energy vs pump energy in atmospheric air.

In atmospheric remote sensing applications, it is the backward lasing that enables single-ended standoff diagnostics. Here, we compare the cascade superfluorescent lasing energy in forward and backward directions. The blue and red solid (dashed) line in Fig. 4 shows the 1409 nm first lasing energy and the 752 nm second lasing energy versus pump energy in the forward (backward) direction, respectively. The error bar is smaller than the marker in the curves. For forward lasing, when the pump energy is lower than 18 μJ, both the first and second lasing show exponential growth with the increase of pump energy, indicating ASE at low pump intensities. When the pump energy exceeds 18 μJ, both the first and second lasing energy show a roughly quadratic relation with the pump energy, and as seen and inferred from Figs. 3(d) and 3(e), the emission transits from ASE to SF. Ideally, for SF emission, the lasing energy should grow as the third power of the pump energy in the absence of losses. Additional experimentation is needed to understand the discrepancy. At highest pump energy, the forward (backward) first and second lasing efficiency respective to the pump energy is 3.2×10^{-5} and 4.0×10^{-5} (1.7×10^{-7} and 0.9×10^{-7}), respectively. The backward lasing energy is about 2 orders of magnitude lower than the forward lasing energy due to the nature of traveling wave excitation in the pumping process, given that the effective gain lifetime (~10 ps) is much shorter than the propagation time over a ~1-cm-long excitation volume. Previous studies [1,2,12] also showed that the backward lasing signal can be even stronger than the forward lasing signal by using longer (nanosecond) pump pulses, which is also confirmed by our simulation results by numerically solving the Maxwell-Bloch equations. In this way, the pump pulse duration is much longer than the propagation time of the excitation volume so that the traveling wave excitation effect can be ignored.

We have analyzed the potential issue of attenuation of the 261 nm radiation propagating through the atmosphere for remote standoff detection at long distances. Our calculations, using normal atmosphere and HITRAN data [42] show that attenuation of 261 nm radiation, including losses and scattering, is approximately 25% for 1 km propagation, i.e., ~75% of the 261 nm pulse energy at low intensity will be delivered at a distance of 1 km. Incidentally, the majority of the attenuation arises from Raleigh scattering.

In conclusion, we have demonstrated bidirectional two-color cascade superfluorescent lasing in Ar in atmospheric air pumped by femtosecond UV pulses at 261 nm and uncovered photon-mediated resonant energy transfer from N_2 to Ar. Time-resolved measurements confirmed that the cascaded lasing arises from SF.

Acknowledgments—We thank Sergei Tochitsky for useful discussions regarding this work. This work was supported by DOE Award No. DE-SC0010064, NSF Grant No. 2003354, and the Office of Naval Research (ONR) Multidisciplinary University Research Initiative (MURI) No. 14-19-1-2517, and the National Natural Science Foundation of China Grant No. 12021004. The computation is completed in the HPC Platform of Huazhong University of Science and Technology.

[1] A. Laurain, M. Scheller, and P. Polynkin, Low-threshold bidirectional air lasing, Phys. Rev. Lett. **113**, 253901 (2014).
[2] A. Dogariu, J. B. Michael, M. O. Scully, and R. B. Miles, High-gain backward lasing in air, Science **331**, 442 (2011).
[3] P. R. Hemmer, R. B. Miles, P. Polynkin, T. Siebert, A. V. Sokolov, P. Sprangle, and M. O. Scully, Standoff spectroscopy via remote generation of a backward-propagating laser beam, Proc. Natl. Acad. Sci. U.S.A. **108**, 3130 (2011).
[4] P. N. Malevich, R. Maurer, D. Kartashov, S. Ališauskas, A. A. Lanin, A. M. Zheltikov, M. Marangoni, G. Cerullo, A. Baltuška, and A. Pugžlys, Stimulated Raman gas sensing by backward UV lasing from a femtosecond filament, Opt. Lett. **40**, 2469 (2015).
[5] Z. Zhang, F. Zhang, B. Xu, H. Xie, B. Fu, X. Lu, N. Zhang, S. Yu, J. Yao, Y. Cheng, and Z. Xu, High-sensitivity gas detection with air-lasing-assisted coherent Raman spectroscopy, Ultrafast Sci. **2022**, 9761458 (2022).
[6] Y. Fu, J. Cao, K. Yamanouchi, and H. Xu, Air-laser-based standoff coherent Raman spectrometer, Ultrafast Sci. **2022**, 9867028 (2022).
[7] N. Zhang, H. Xie, H. Zhang, X. Lu, Y. Chen, Y. Wu, Y. Cheng, and J. Yao, Electronic-resonance-enhanced coherent Raman spectroscopy with a single femtosecond laser beam, Laser Photonics Rev. **17**, 2300020 (2023).
[8] J. Yao, B. Zeng, H. Xu, G. Li, W. Chu, J. Ni, H. Zhang, S. L. Chin, Y. Cheng, and Z. Xu, High-brightness switchable multiwavelength remote laser in air, Phys. Rev. A **84**, 051802(R) (2011).
[9] H. Zhang, C. Jing, J. Yao, G. Li, B. Zeng, W. Chu, J. Ni, H. Xie, H. Xu, S. L. Chin, K. Yamanouchi, Y. Cheng, and Z. Xu, Rotational coherence encoded in an "air-laser" spectrum of nitrogen molecular ions in an intense laser field, Phys. Rev. X **3**, 041009 (2013).
[10] Y. Liu, P. Ding, G. Lambert, A. Houard, V. Tikhonchuk, and A. Mysyrowicz, Recollision-induced superradiance of ionized nitrogen molecules, Phys. Rev. Lett. **115**, 133203 (2015).
[11] H. Xu, E. Lötstedt, A. Iwasaki, and K. Yamanouchi, Sub-10-fs population inversion in N_2^+ in air lasing through multiple state coupling, Nat. Commun. **6**, 8347 (2015).
[12] A. Dogariu and R. B. Miles, Three-photon femtosecond pumped backwards lasing in argon, Opt. Express **24**, A544 (2016).
[13] J. Yao, S. Jiang, W. Chu, B. Zeng, C. Wu, R. Lu, Z. Li, H. Xie, G. Li, C. Yu, Z. Wang, H. Jiang, Q. Gong, and Y. Cheng, Population redistribution among multiple electronic states of molecular nitrogen ions in strong laser fields, Phys. Rev. Lett. **116**, 143007 (2016).
[14] *Air Lasing*, edited by P. Polynkin and Y. Cheng, Springer Series in Optical Sciences Vol. 208 (Springer International Publishing, Cham, 2018).
[15] L. Yuan, Y. Liu, J. Yao, and Y. Cheng, Recent advances in air lasing: A perspective from quantum coherence, Adv Quantum Technol. **2**, 1900080 (2019).
[16] T. Ando, E. Lötstedt, A. Iwasaki, H. Li, Y. Fu, S. Wang, H. Xu, and K. Yamanouchi, Rotational, vibrational, and electronic modulations in n_2^+ lasing at 391 nm: Evidence of coherent $B^2\Sigma_U^+ - X^2\Sigma_g^+ - A^2\Pi_u$ coupling, Phys. Rev. Lett. **123**, 203201 (2019).
[17] R. Danylo, X. Zhang, Z. Fan, D. Zhou, Q. Lu, B. Zhou, Q. Liang, S. Zhuang, A. Houard, A. Mysyrowicz, E. Oliva, and Y. Liu, Formation dynamics of excited neutral nitrogen molecules inside femtosecond laser filaments, Phys. Rev. Lett. **123**, 243203 (2019).
[18] H. Li, M. Hou, H. Zang, Y. Fu, E. Lötstedt, T. Ando, A. Iwasaki, K. Yamanouchi, and H. Xu, Significant enhancement of N 2 + lasing by polarization-modulated ultrashort laser pulses, Phys. Rev. Lett. **122**, 013202 (2019).
[19] H. Li, E. Lötstedt, H. Li, Y. Zhou, N. Dong, L. Deng, P. Lu, T. Ando, A. Iwasaki, Y. Fu, S. Wang, J. Wu, K. Yamanouchi, and H. Xu, Giant enhancement of air lasing by complete population inversion in N 2 +, Phys. Rev. Lett. **125**, 053201 (2020).
[20] M. Richter, M. Lytova, F. Morales, S. Haessler, O. Smirnova, M. Spanner, and M. Ivanov, Rotational quantum beat lasing without inversion, Optica **7**, 586 (2020).
[21] X. Zhang, Q. Lu, Z. Zhang, Z. Fan, D. Zhou, Q. Liang, L. Yuan, S. Zhuang, K. Dorfman, and Y. Liu, Coherent control of the multiple wavelength lasing of N_2^+: Coherence transfer and beyond, Optica **8**, 668 (2021).
[22] C. Kleine, M.-O. Winghart, Z.-Y. Zhang, M. Richter, M. Ekimova, S. Eckert, M. J. J. Vrakking, E. T. J. Nibbering, A. Rouzée, and E. R. Grant, Electronic state population dynamics upon ultrafast strong field ionization and fragmentation of molecular nitrogen, Phys. Rev. Lett. **129**, 123002 (2022).
[23] C. Zhuang, X. Zhang, Q. Lu, and Y. Liu, Optical amplification and gain dynamics of cavity-free lasing of argon pumped by ultraviolet femtosecond pulses, Opt. Express **30**, 17156 (2022).

[24] A. Dogariu and R. B. Miles, Remote backward-propagating lasing of nitrogen and oxygen in air, in *CLEO: 2015*(OSA, San Jose, California, 2015), p. SM1N.1.
[25] A. Dogariu and R. B. Miles, Backwards lasing in atmospheric air from argon, in *Conference on Lasers and Electro-Optics* (OSA, San Jose, California, 2018), p. JTh5B.8.
[26] S. W. Grib, H. U. Stauffer, S. Roy, and S. A. Schumaker, Resonance-enhanced, rare-gas-assisted femtosecond-laser electronic-excitation tagging in argon/nitrogen mixtures, Appl. Opt. **60**, C32 (2021).
[27] J. B. Michael, M. R. Edwards, A. Dogariu, and R. B. Miles, Femtosecond laser electronic excitation tagging for quantitative velocity imaging in air, Appl. Opt. **50**, 5158 (2011).
[28] R. H. Dicke, Coherence in spontaneous radiation processes, Phys. Rev. **93**, 99 (1954).
[29] J. J. Maki, M. S. Malcuit, M. G. Raymer, R. W. Boyd, and P. D. Drummond, Influence of collisional dephasing processes on superfluorescence, Phys. Rev. A **40**, 5135 (1989).
[30] L. S. Cederbaum, J. Zobeley, and F. Tarantelli, Giant intermolecular decay and fragmentation of clusters, Phys. Rev. Lett. **79**, 4778 (1997).
[31] R. Santra, J. Zobeley, L. S. Cederbaum, and N. Moiseyev, Interatomic Coulombic decay in van der Waals clusters and impact of nuclear motion, Phys. Rev. Lett. **85**, 4490 (2000).
[32] V. Averbukh, I. B. Müller, and L. S. Cederbaum, Mechanism of interatomic Coulombic decay in clusters, Phys. Rev. Lett. **93**, 263002 (2004).
[33] T. Jahnke, A. Czasch, M. S. Schöffler, S. Schössler, A. Knapp, M. Käsz, J. Titze, C. Wimmer, K. Kreidi, R. E. Grisenti, A. Staudte, O. Jagutzki, U. Hergenhahn, H. Schmidt-Böcking, and R. Dörner, Experimental observation of interatomic Coulombic decay in neon dimers, Phys. Rev. Lett. **93**, 163401 (2004).
[34] See Supplemental Material at http://link.aps.org/supplemental/10.1103/PhysRevLett.133.063201 for experimental setup and more experimental data.
[35] K. Kitano and H. Maeda, Cascade and yoked superfluorescence detected by sum frequency generation spectroscopy, Opt. Lett. **48**, 69 (2023).
[36] J. H. Brownell, X. Lu, and S. R. Hartmann, Yoked superfluorescence, Phys. Rev. Lett. **75**, 3265 (1995).
[37] J. T. Verdeyen, *Laser Electronics*, 3rd ed., Prentice Hall Series in Solid State Physical Electronics (Prentice Hall, Englewood Cliffs, N.J, 1995).
[38] S. Kunze, R. Groll, B. Besser, and J. Thöming, Molecular diameters of rarefied gases, Sci. Rep. **12**, 2057 (2022).
[39] G. Grynberg, Three-photon absorption: Selection rules and line intensities, J. Phys. (Les Ulis, Fr.) **40**, 965 (1979).
[40] D. J. Jackson and J. J. Wynne, Interference effects between different optical harmonics, Phys. Rev. Lett. **49**, 543 (1982).
[41] M. G. Payne, W. R. Garett, and H. C. Baker, Effects of collective emission on multiphoton excitation and ionization near a three-photon resonance, Chem. Phys. Lett. **75**, 468 (1980).
[42] I. Gordon *et al.*, The HITRAN2020 molecular spectroscopic database, J. Quantum Spectrosc. Radiat. Transf. **277**, 107949 (2022).